

Thermal Elastohydrodynamic Lubrication Analysis of High-Speed and Light-Load Rolling Bearing with Double Rings Rotation

Junning LI*, Ka HAN, Qian WANG, Wuge CHEN, Jiafan XUE

Abstract: In order to reveal the lubrication performance of the rolling bearing under the condition of double rings rotation, a novel rolling bearing contact lubrication analysis model for double rings rotation with an improved load distribution is developed. The effects of different parameters, such as the load, slip and speed, on the distribution of the temperature, pressure and film thickness of the rolling bearing are studied. The results show that the change rate of speed in double rings homonymous rotation is greater than that for single ring rotation and double rings reverse rotation on the inner and outer rings. Thus, the temperature change is higher for the former rotation than the latter two rotations. The oil film thickness for double rings reverse rotation is less than that for the other two types of rotations. The pressure distribution for the three types of rotations is more complex than the behaviour of the contact velocity and film. For variable speed, the temperature of the reverse rotation increases with the inner ring speed, which decreases as the outer ring speed increases. The temperature increases with the inner ring speed, which increases with the outer ring speed. The temperature of the double rings homonymous rotation or the reverse rotation increases with the load and slip. This manuscript can serve as a reference for research on the life and reliability of helicopter engine bearings under various rotation conditions.

Keywords: double rings rotation; high speed; light load; lubrication performance: rolling bearing; slip

1 INTRODUCTION

A rolling bearing is one of the most widely used components in rotating machinery, whose running state directly affects the accuracy, reliability and service life of the whole machine [1]. In helicopter, to improve the energy efficiency and compactness of the engine structures, a dual-rotor system has been widely employed. Frictional heating in high-speed bearings has been one of the primary factors in the failure of the main shaft bearing in helicopter engine [2-3]. Modern aero-engine spindle shafts mostly adopt a double-rotor structure, which forms a coupling between the low-pressure rotor and the high-pressure rotor, and the bearings connecting the high-low pressure rotor are the intermediate bearings [4]. In normal operation, the inner and outer rings of the inter-shaft bearing run at the same time. The engine structure makes it extremely difficult to lubricate the inter-shaft bearing. Therefore, it is of great significance to analyse the lubrication of the inter-shaft bearing. An integral calculation method for the frictional heat generation of rolling bearings is presented by Palmgren [5], which is suitable for low-speed, light-load and good lubrication conditions. Gao [6] proposes a new theoretical method to investigate the thermal behaviours of the inter-shaft bearing considering the nonlinear dynamic characteristics of a dual-rotor system by combining heat transfer and nonlinear dynamics. Wang [7-8] analyses the dynamic characteristics of a dual-rotor system with an inter-shaft bearing and performed a theoretical analysis and an experimental study on the vibrational response characteristics of a dual-rotor with imbalance-misalignment coupling faults. In order to reduce cross-excitation between the low pressure and the high-pressure shafts of two spool rotor, Gupta [9] proposes some designs of inter-shaft bearing with squeeze film. Jiang [10] considers the variable speed of dual rotors, as well as the weak signal, and uses linear prediction, spectral kurtosis, and order tracking in the rotational speed difference domain to develop a fault feature extraction scheme for the weak fault signals of inter-shaft bearings. Tian [11] accurately describes the dynamic features of inter-shaft bearings with localized defects in operation. Guskov [12] uses a rather fine numerical model to predict

experimentally observed phenomena for a dual rotor test rig. The thermal elastohydrodynamic lubrication theory can be used to analyse the minimum oil film thickness, pressure distribution and local oil film temperature distribution in the key contact pair of bearings by including an energy equation and upper and lower boundary temperature conditions based on isothermal elastic lubrication. The lubricating oil film can separate the rolling raceway from the contact raceway. The viscosity of the lubricant causes the oil film to be subjected to viscous shear forces and the extrusion pressure of the fluid, thereby generating heat and increasing the temperature of the oil film. As a result, heat is transferred from the high-temperature environment to the bearing, increasing the temperature. R. Kumar [13] reviews the experimental methods that have been applied to date for measuring oil film thickness and pressure. The lubricating oil is regarded by Doki-Thonon [14-15] as a non-Newtonian fluid, and thermal elastohydrodynamic lubrication is applied to the thermal analysis of a rolling bearing. Huang [16] performs a comparative analysis of the line contact multigrid method and the Newton iteration method. The results show that the multigrid method is convergent and fast. Popinceau [17] correlates the fatigue life of rolling bearings using the trends indicated by the EHL theory and tests a large number of identical ball bearings over a range of rolling speeds, using various mineral oils and greases as lubricants. Corrections to the classical equation for the prediction of rolling bearing life are proposed.

In addition to the studies discussed above, researchers have achieved remarkable advances in the field of rolling bearings; however, most of these theories did not include distribution laws for the temperature rise, pressure and oil film thickness in the critical contact area under different rotation conditions for double rings rotation in helicopter engine bearing. Slip has rarely been included in analysing the temperature rise distribution in condition of double rings rotation. Therefore, in this manuscript, we compared and analysed the lubrication performance of key contact pairs of rolling bearings under different loads, slip rates, rotation speeds and rotation states by introducing different motion parameters and using the thermal

elastohydrodynamic calculation program for different double rings rotation states.

2 MATHEMATICAL MODEL

2.1 Kinematics Analysis Model

To determine the rotational speed of a rolling element and a cage considering load conditions, the following assumptions need to be adopted before deducing the simple kinematics of the rolling bearing: 1) The bearing element is a rigid body, and the influence of contact deformation is neglected; 2) The effect of radial clearance is neglected; 3) The rolling element purely on the ring raceway without sliding; and 4) The action of the oil film is neglected [18].

The case of a cylindrical roller bearing is used as an example to derive the angular velocity of the bearing cage, the rotational angular velocity of the rolling element and the average velocity. The simple motion relationship of a rolling bearing is shown in Fig. 1. The clockwise rotation direction is considered to be positive, and the counterclockwise rotation direction is considered to be negative.

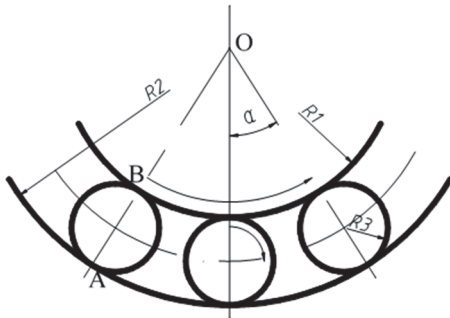


Figure 1 Kinematics relationship of a roller bearing

1) The theoretical angular velocity of the cage
The inner raceway B has a velocity of:

$$v_B = \frac{\pi n_i}{30} R_1 \quad (1)$$

Consider point A to be the instantaneous center of velocity and that the velocity of the roller point B is:

$$v_B = 2\omega_1 R_3 \quad (2)$$

In the formula given below, R_1 is the inner ring raceway radius (m), R_3 is the roller radius (m), n_i is the inner ring speed (r/min), and (1) is the angular velocity of the roller relative to point A (rad/s).

$$\omega_1 = \frac{\pi n_i R_1}{60 R_3} \quad (3)$$

The point speed v_{O1} of the roller center O_1 is:

$$v_{O1} = \omega_1 R_3 = \omega_c (R_1 + R_3) \quad (4)$$

$$\omega_c = \frac{\pi n_i R_1}{60(R_1 + R_3)} = \frac{\pi n_i}{60} \left(1 - \frac{D_r}{D_m}\right) \quad (5)$$

$$n_c = \frac{n_i}{2} \left(1 - \frac{D_r}{D_m}\right) \quad (6)$$

In the formula, ω_c is the angular velocity of the cage (rad/s), D_r is the diameter of the roller (m), and D_m is the diameter of the bearing pitch circle (m).

2) The theoretical rotational angular velocity of a rolling element

When the center of the roll is fixed and the speed of the roller n_r is zero, the retainer speed relative to that of the inner ring n_{ci} is:

$$n_{ci} = n_c - n_i \quad (7)$$

The relative sliding of the contact point is not considered, that is, the linear velocity of the rolling element at the contact point is equal to the linear velocity of the inner ring raceway. The rotational speed of the rolling element around its own axis can be expressed as:

$$D_r n_r = D_i n_{ci} \quad (8)$$

D_i is the raceway radius of the inner ring (m). Substituting Eq. (6) and (7) into Eq. (8) allows the theoretical rotational speed and the angular velocity of the roller around its axis to be deduced:

$$n_r = -\frac{n_i D_m}{2 D_r} \left[1 - \left(\frac{D_r}{D_m}\right)\right]^2 \quad (9)$$

$$\omega_r = -\frac{\pi n_i D_m}{60 D_r} \left[1 - \left(\frac{D_r}{D_m}\right)\right]^2 \quad (10)$$

3) The average speed at the contact point between the roller and the ring raceway

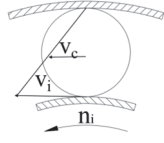
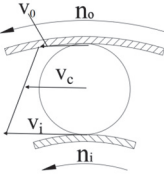
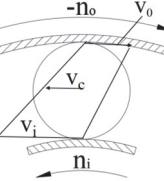
The average velocity of the contact point can be expressed as:

$$\bar{u} = \frac{1}{2} (D_m - D_r) (\omega_i - \omega_c) = \frac{\pi}{30} (n_i - n_c) \left(\frac{D_m}{2} - \frac{D_r}{2}\right) \quad (11)$$

Similarly, under pure rolling conditions, the rotational speed of the cage and the rolling element under various rotating conditions of the two rings in rolling bearing can be obtained, as shown in Tab. 1.

Previously, frictional thermal analysis of a rolling bearing is mainly carried out when the outer ring is held fixed and the inner ring is rotated. In this manuscript, the theory of single ring rotation and analytical methods from the reference [19] are used to develop a frictional thermal analysis model of a rolling bearing with a slip factor for two rings rotating simultaneously. Using the case of a NU210 roller bearing as an example, the temperature rise curves of each layer on the contact surface between the roller and inner ring are calculated using the program when double rings rotate simultaneously.

Table 1 Rotational speed of the cage and the rolling element under various rotating conditions

Rotating conditions	Schematic diagram	Cage speed n_c / r/min	Roll element speed n_r / r/min
Inner ring rotation		$n_i K_1$	$-n_i \times \frac{2D_m K_1 K_2}{D_r}$
Double rings homonymous rotation		$n_i K_1 + n_o K_2$	$(n_i - n_o) \times \frac{2D_m K_1 K_2}{D_r}$
Double rings reverse rotation		$n_i K_1 - n_o K_2$	$-(n_i - n_o) \times \frac{2D_m K_1 K_2}{D_r}$

The load distribution is calculated using the modified load calculation method, and the resulting value for the maximum contact load is used as an input into the thermal elastohydrodynamic calculation program as a "contact load" to calculate the temperature and the oil film pressure distribution.

2.2 Thermal Elastohydrodynamic Lubrication Model

1) Governing equation for temperature

The energy equation [20] for a line contact thermal elastohydrodynamic lubrication problem may be written as follows:

$$\rho c_p u \frac{\partial T}{\partial x} + \frac{T}{\rho} \frac{\partial p}{\partial T} \left(u \frac{\partial p}{\partial x} \right) - k \frac{\partial^2 T}{\partial z^2} = \eta \left(\frac{\partial u}{\partial z} \right)^2 \quad (12)$$

c_p is the isobaric specific heat of the fluid and k is the thermal conductivity of the fluid. The upper and lower boundary temperature conditions must be specified as follows:

$$\left. \begin{aligned} T(x, 0) &= \frac{k}{\sqrt{\pi \rho_1 c_1 k_1 u_1}} \int_{-\infty}^x \frac{\partial T}{\partial z} \Big|_{x,0} \frac{ds}{\sqrt{x-s}} + T_0 \\ T(x, h) &= \frac{k}{\sqrt{\pi \rho_2 c_2 k_2 u_2}} \int_{-\infty}^x \frac{\partial T}{\partial z} \Big|_{x,h} \frac{ds}{\sqrt{x-s}} + T_0 \end{aligned} \right\} \quad (13)$$

2) Reynolds equation

$$\frac{d}{dx} \left(\frac{\rho h^3}{\eta} \frac{dp}{dx} \right) = 12U \frac{d(\rho h)}{dx} \quad (14)$$

3) Film thickness equation

$$h(x) = h_0 + \frac{x^2}{2R} - \frac{2}{\pi E} \int_{s_1}^{s_2} p(s) \ln(s-x)^2 ds + c \quad (15)$$

After dimensional normalization, the above equation becomes:

$$H(X) = H_0 + \frac{X^2}{2} - \frac{1}{\pi} \int_{X_0}^{X_c} \ln |X - X'|^2 P(X') dX' \quad (16)$$

H_0 is an infinite number of unknowns whose value is obtained in the solution process.

4) Viscosity-temperature equation

$$\eta = \eta_0 \exp \left\{ (\ln \eta_0 + 9.67) [(1+p/p_0)^z \left(\frac{T-138}{T_0-138} \right)^{-1.1} - 1] \right\} \quad (17)$$

5) Pressure-temperature equation

$$\rho = \rho_0 \left(1 + \frac{0.6p}{1+1.7p} + D(T-T_0) \right) \quad (18)$$

6) Load equation

$$\int_{x_{in}}^{x_{out}} p(x) dx = W \quad (19)$$

Let the load W applied per unit length be a constant, and dimensional normalizing of the load Eq. (19) yields:

$$\int_{X_{in}}^{X_{out}} P(X) dX = \frac{\pi}{2} \quad (20)$$

2.3 Average Velocities of Double Rings and Single Ring

The basic parameters for the roller bearing are shown in Tab. 2. The initial value of the dimensional normalization coordinates is taken to be $X_{in} = -4$, and the final value of the dimensional normalization coordinates is taken to be $X_{out} = 1.4$.

Table 2 Basic parameters of a NU210 cylindrical roller bearing

Roller number	Roller diameter / mm	Roller length / mm	Inner ring diameter / mm	Outer ring diameter / mm	Pitch diameter / mm	Bearing width / mm	Cage diameter / mm
16	13	13	50	90	70	20	75

Table 3 Operating condition parameters of a NU210 cylindrical roller bearing

Dynamic viscosity of lubricating oil / Pa·s	Comprehensive modulus of elasticity / Pa	Slip factor	Radial load / N	Inner ring speed / r/min	Outer ring speed / r/min	Initial temperature / °C	Inlet oil temperature / °C
0.015	2.25E11	0.2	2000	12000	10000	40	40

Combing with Tab. 1 and Eq. (11), the average velocity of the contact area for the double rings homonymous rotation, double rings reverse rotation and single ring rotation can be calculated and obtained.

2.4 Numerical Scheme

The method for calculating the load distribution is modified to obtain the maximum unit load in the contact area, and the average velocity in the contact area is obtained by kinematics analysis.

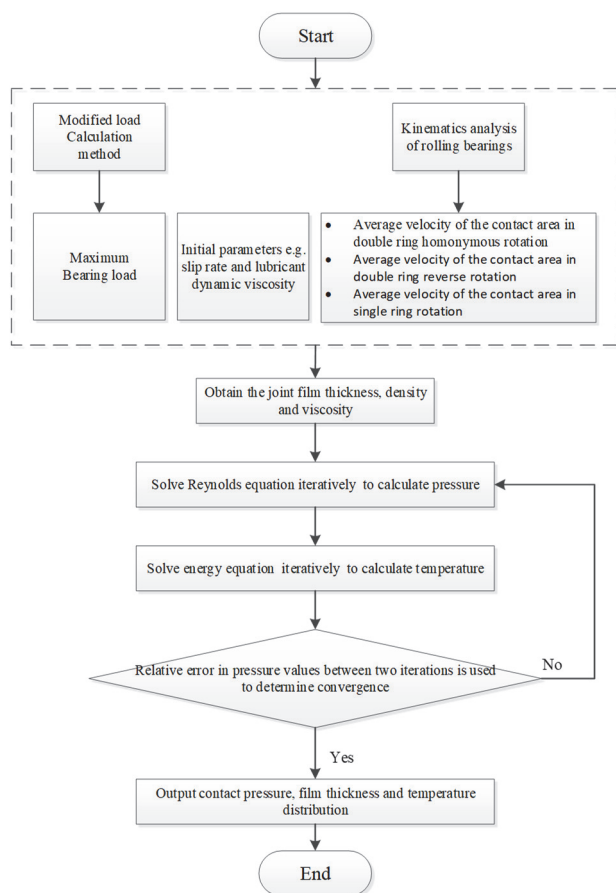


Figure 2 Flowchart of numerical analysis

The slip rate and the lubricant dynamic viscosity are taken into account to calculate the film thickness, density

and viscosity. A new generation of equations is then substituted into the Reynolds equation for the stress distribution using the pressure value from the previous iteration, and the energy equation is then solved for the temperature distribution, using the newly generated temperature and viscosity. A new iteration is performed to obtain the pressure again and this process is iterated until there is relative error convergence between the last two iterated pressure values. Finally, the following results are obtained for the bearing zone: the inner ring raceway roller contact pressure distribution, the film thickness distribution and the temperature distribution. A detailed flowchart of numerical analysis is shown in Fig. 2.

3 RESULTS AND DISCUSSION

In the following figures, the parameters on both abscissas are dimensionless. Fig. 3 and Fig. 4 indicate the distribution of the temperature rise in each layer of contact line thermal elastohydrodynamic flow. It can be seen that the temperature distribution does not change much for $X \leq -1$. When $X > -1$, the temperature of each layer first increases then decreases, and then reaches a plateau for $X > 1$. As the oil film thickness decreases, the pressure increases sharply. Under the action of the shear extrusion force, the oil film thickness increases sharply, resulting in a sharp rise in temperature.

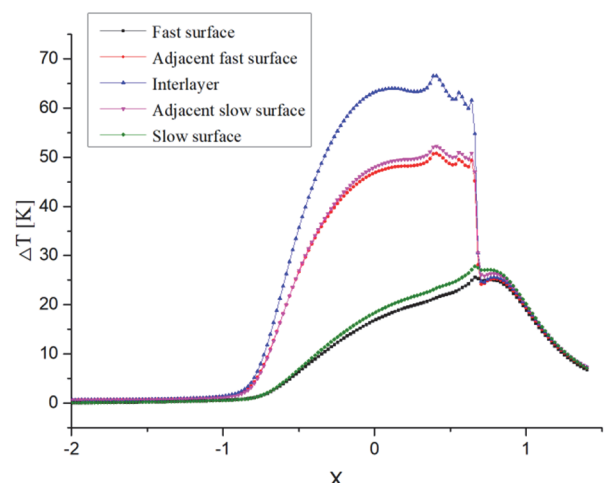


Figure 3 Temperature rise distribution in each layer for homonymous rotation

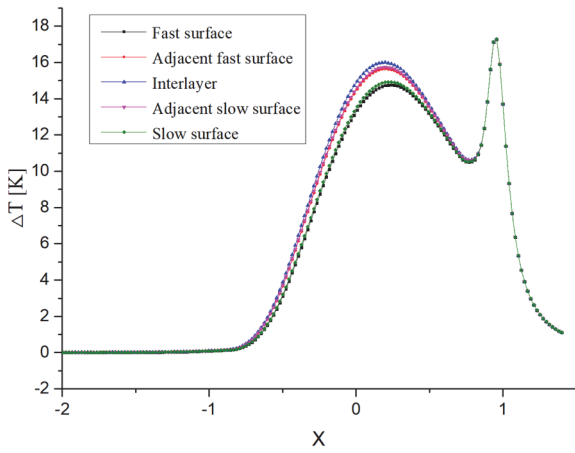


Figure 4 Temperature rise distribution in each layer for reverse rotation

The temperature of the outlet area is higher than that of the inlet area because the thickness of the oil film in the outlet area is thinner than that in the inlet area. Thus, the fluid in the outlet area is subject to a greater shear force than that in the inlet area, resulting in higher frictional heat. Second, the lubricant in the inlet area is cold oil, whereas the lubricant in the outlet area is hot oil.

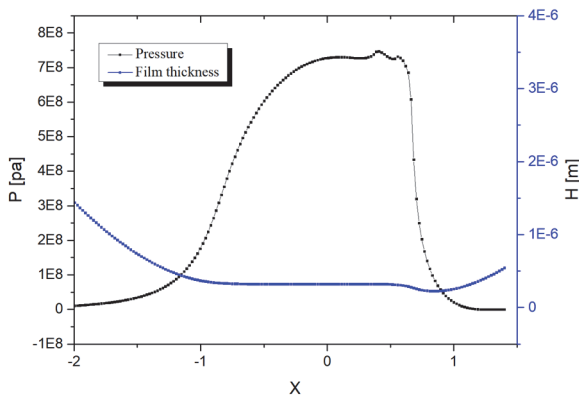


Figure 5 Distribution of film thickness and pressure for reverse rotation

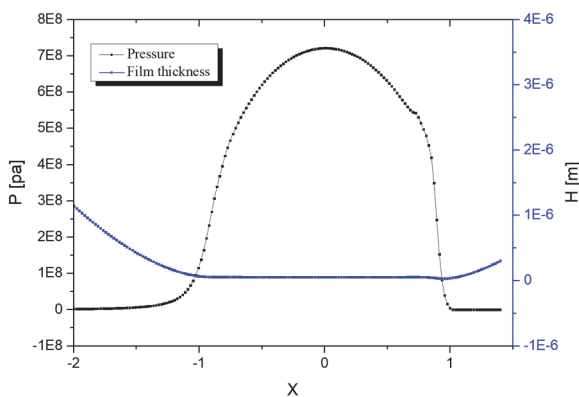


Figure 6 Distributions of film thickness and pressure for homonymous rotation

Fig. 5 and Fig. 6 show the distribution of the film thickness and the pressure for line contact thermal elastohydrodynamic flow. The pressure distribution in the inlet area increases gradually under the action of the fluid dynamic pressure, where the pressure distribution in the contact area is similar to the Hertz distribution curve, and the pressure in the outlet area decreases sharply to the environmental pressure. The oil film thickness distribution decreases as the contact pressure increases, and the

minimum film thickness appears between $X = -1 \sim 1$. The oil film shape for the rest of the contact area is roughly parallel.

3.1 Lubrication Characteristics under Different Rotation Conditions

Fig. 7 and Fig. 8 correspond to a slip rate of 0.2. The distributions of the temperature rise and the film thickness for the middle layer are compared in the same direction for single ring rotation and homonymous and reverse rotation for the double rings. The relative velocity of the double rings homonymous rotation is larger than that for the single ring rotation, thus, the temperature rise is higher and the oil film is thicker for the former rotation than for the latter rotation. The relative velocity of the double rings reverse rotation is lower than that of the single ring rotation, thus, the temperature rise is lower and the oil film is thinner for the former rotation compared to the latter rotation.

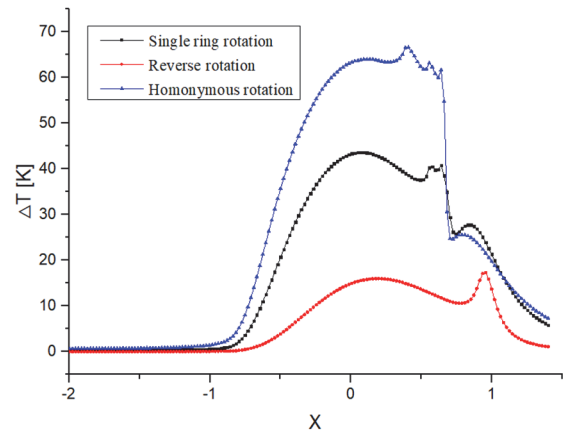


Figure 7 Temperature rise distributions under different rotation conditions

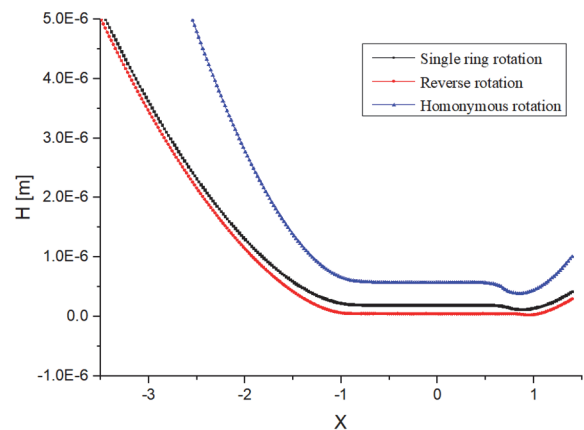


Figure 8 Film thickness distributions under different rotation conditions

Fig. 9 compares the pressure distribution for single ring rotation, double rings homonymous rotation and double rings reverse rotation. It can be seen that the pressure distribution is relatively complex under this operating condition because the relatively large rotational speed at the contact point brings in more oil, which increases the pressure in the inlet area, followed by a section where the pressure grows in a stable manner. After the accumulation of the oil film briefly increases the pressure at the outlet, the pressure distribution decreases sharply due to the quick release speed.

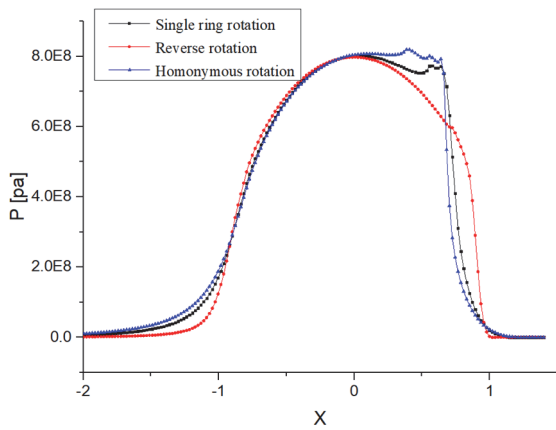


Figure 9 Pressure distributions under different rotation conditions

3.2 Temperature Rise Distribution under Different Slip Factors

Fig. 10 and Fig. 11 compare the temperature rise distributions for two rotations with slip factors of $s = 0.1, 0.3, 0.5$ and 0.7 . The radial load is $F_r = 2000$ N. The inner ring speed $n = 10000$ r/min. The oil temperature of the oil film increases with the increase in the different slip factors, and the temperature rise for the double rings rotation is higher than that for the reverse rotation.

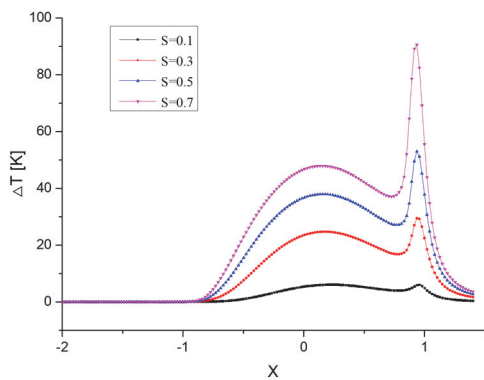


Figure 10 Temperature rise distribution for reverse rotation with different slip factors

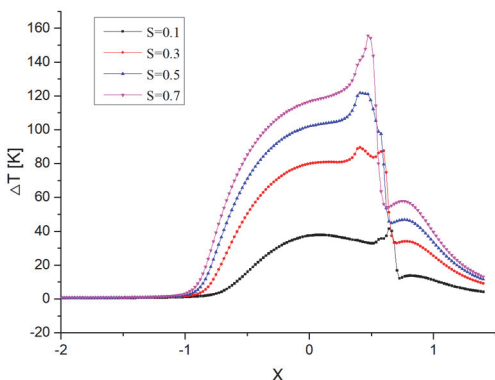


Figure 11 Temperature rise distribution for homonymous rotation with different slip factors

3.3 Temperature Rise Distribution under Different Rotational Speeds

In Fig. 12 and Fig. 13, the inner ring speed of the rolling bearing is 12000 r/min, and the outer ring speed is

-10000 r/min. The change in the temperature rise is shown for the condition where the outer and inner rings have invariant speeds for double rings homonymous and reverse rotation. For the case of double rings reverse rotation, the temperature increases with the inner ring speed and decreases as the outer ring speed increases. For double rings homonymous rotation, the temperature rise increases with the inner ring speed and with the outer ring speed.

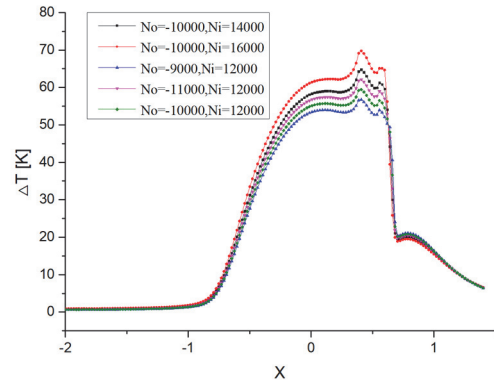


Figure 12 Temperature rise distribution under reverse rotation with variable speed

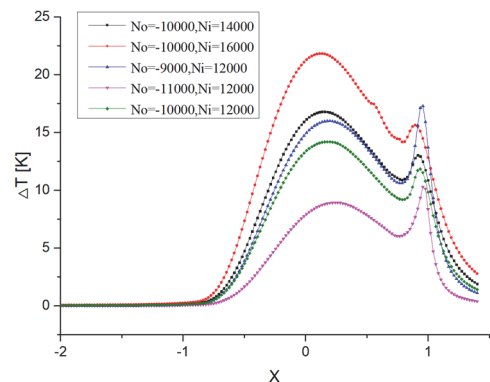


Figure 13 Temperature rise distribution under homonymous rotation with variable speed

3.4 Temperature Rise Distribution under Different Loads

Fig. 14 and Fig. 15 compare the temperature rise distributions for a slip factor $s = 0.2$, radial loads of $F_r = 1000$ N, 2000 N, and 3000 N, and an inner ring speed $n = 10000$ r/min. The temperature of the oil film increases with the load, and the temperature rise for double rings homonymous rotation is higher than that for reverse rotation.

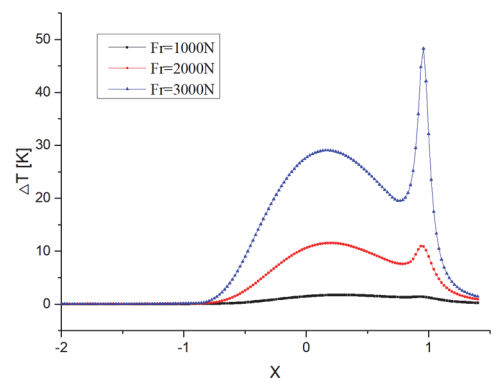


Figure 14 Temperature rise distributions for reverse rotation under different loads

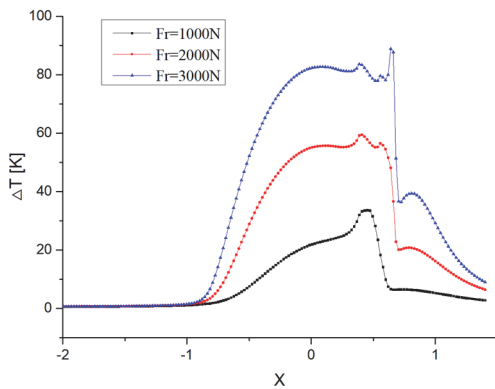


Figure 15 Temperature rise distributions for homonymous rotation under different loads

3.5 Model Verification

In reference [21], it is found that the shape of the pressure distribution curve changes obviously with the bearing speed at the contact point under rotation and gradually deviates from a Hertzian distribution. For small velocities, a secondary pressure peak is observable. As the velocity increases, the secondary pressure peak almost disappears, and the position of the maximum pressure gradually moves towards the entrance area. The oil film thickness also increases and the ratio of the necking portion to the total contact width increases with the velocity. This phenomenon is basically in agreement with the trends for the oil film and pressure distribution that are reported in this paper, which verifies the rationality of the model.

4 CONCLUSIONS

This manuscript has focused on the contact lubrication performance of high-speed and light-load rolling bearings under different rotation conditions for double rings. The results show that the change in the contact velocity between the roller and the inner ring under homonymous rotation of the inner and outer rings is higher than that for reverse rotation, and the change in the temperature rise is more obvious for the former case than for the latter case. The oil film thickness is less than that of double rings homonymous rotation and single ring rotation. The temperature rise for double rings homonymous rotation or reverse rotation exhibits an upward trend with increasing loads and slip rates.

The research has significance for the reliability analysis of the double rings rotating rolling bearings and can serve as a reference for studying bearing-rotor system reliability and stability under the unique conditions of double-elements rotation, such as those that occur in helicopter engines.

Acknowledgments

This work was supported in part by the Program of State Key Laboratory of Mechanical Transmissions under Grant SKLMT-KFKT-201808, National Natural Science Foundation of China under Grant 51505361 and Grant 51975448, Innovative Talents Promotion Plan in Shaanxi Province under Grant 2017KJXX-58.

5 REFERENCES

- [1] Wang, H., Li, R., Tang, G., Yuan, H. et al. (2014). A Compound Fault Diagnosis for Rolling Bearings Method Based on Blind Source Separation and Ensemble Empirical Mode Decomposition. *PLOS ONE*, 9(10). <https://doi.org/10.1371/journal.pone.0109166>
- [2] Gloeckner, P. & Franz-Josef, E. (2010). Micro-sliding in high-speed aircraft engine ball bearings. *Tribology transactions*, 53(3), 369-375. <https://doi.org/10.1080/10402000903312364>
- [3] Pang, L., Luo, K., Yuan, Y. et al. (2019). Thermal Performance of Helicopter Air Conditioning System with Lube Oil Source (LOS) Heat Pump. *Energy*, 190, 116446. <https://doi.org/10.1016/j.energy.2019.116446>
- [4] Lin, J. & Zhang, Z. (2001). Prospects of aero-engine power transmission system in the 21st century. *Journal of Aerospace Power*, 16(1), 108-114.
- [5] Pamlgren, A. (1959). *Ball and Roller Bearing*. 3rd ed. Burbank: Philadelphia.
- [6] Gao, P., Chen, Y., & Hou, L. (2020). Nonlinear thermal behaviors of the inter-shaft bearing in a dual-rotor system subjected to the dynamic load. *Nonlinear Dynamics*, 101(1), 191-209. <https://doi.org/10.1007/s11071-020-05753-w>
- [7] Wang, N., Jiang, D., & Xu, H. (2019). Dynamic characteristics analysis of a dual-rotor system with inter-shaft bearing. *Proceedings of the Institution of Mechanical Engineers, Part G: Journal of Aerospace Engineering*, 233(3), 1147-1158. <https://doi.org/10.1177/0954410017748969>
- [8] Wang, N. & Jiang, D. (2018). Vibration response characteristics of a dual-rotor with unbalance-misalignment coupling faults: Theoretical analysis and experimental study. *Mechanism and Machine Theory*, 125, 207-219. <https://doi.org/10.1016/j.mechmachtheory.2018.03.009>
- [9] Gupta, K. & Chatterjee, S. (2014). Experimental Investigations of Inter Shaft Squeeze Film Dampers for Two-Spool Aero Gas Turbine Rotor. *Nachrichten Aus Chemie Technik Und Laboratorium*, 2(5), 433-440. <https://doi.org/10.1002/nadc.19800280812>
- [10] Jiang, Z., Hu, M., Feng, K. et al. (2017). Weak fault feature extraction scheme for intershaft bearings based on linear prediction and order tracking in the rotation speed difference domain. *Applied Sciences*, 7(9), 937. <https://doi.org/10.3390/app7090937>
- [11] Tian, J., Ai, Y., Fei C. et al. (2019). Dynamic modeling and simulation of inter-shaft bearings with localized defects excited by time-varying displacement. *Journal of Vibration and Control*, 25(8), 1436-1446. <https://doi.org/10.1177/1077546318824927>
- [12] Guskov, M., Sinou, J. J., Thouverez, F. et al. (2007). Experimental and numerical investigations of a dual-shaft test rig with intershaft bearing. *International Journal of Rotating Machinery*, 2007, 1-12. <https://doi.org/10.1155/2007/75762>
- [13] Kumar, R., Azam, M. S., Ghosh, S. K. et al. (2018). 70 years of Elastohydrodynamic Lubrication (EHL): A Review on Experimental Techniques for Film Thickness and Pressure Measurement. *MAPAN*, 33(4), 481-491. <https://doi.org/10.1007/s12647-018-0277-1>
- [14] Doki-Thonon, T., Fillot, N., Vergne, P. et al. (2012). Numerical insight into heat transfer and power losses in spinning EHD non-Newtonian point contacts. *Proceedings of the Institution of Mechanical Engineers Part J: Journal of Engineering Tribology*, 226, 23-35. <https://doi.org/10.1177/1350650111419567>
- [15] Doki-Thonon, T., Fillot, N., Morales Espejel, G. E. et al. (2013). A Dual Experimental/Numerical Approach for Film Thickness Analysis in TEHL Spinning Skewing Circular Contacts. *Tribology Letters*, 50(1), 115-126. <https://doi.org/10.1007/s11249-013-0122-1>

- [16] Huang, P. & Wen, S. (1992). Study on oil film and pressure distribution of micro-EHL. *Journal of Tribology*, 114(1), 42-46. <https://doi.org/10.1115/1.2920865>
- [17] Popinceanu, N. G., Gafițanu, M. D., Crețu, S. S. et al. (1977). Rolling bearing fatigue life and EHL theory. *Wear*, 45(1), 17-32. [https://doi.org/10.1016/0043-1648\(77\)90099-0](https://doi.org/10.1016/0043-1648(77)90099-0)
- [18] Wan, C. (1987). *Analysis method of rolling bearing*. China machine press: Beijing.
- [19] Boncompain, R., Fillon, M., & Frene, J. (1986). Analysis of thermal effects in hydrodynamic bearings. *Journal of Tribology*, 108(2), 219-224. <https://doi.org/10.1115/1.3261166>
- [20] Huang, P. (2013). *Numerical calculation method of elastohydrodynamic lubrication*. Tsinghua University press: Beijing.
- [21] Liu, Y. & Gao, C. (2008). Numerical analysis of thermal elastohydrodynamic lubrication of rolling bearing. *Mechanical engineering and automation*, (1), 34-36.

Contact information:

Junning LI, Ass. Prof., Mechanical Engineering
(Corresponding author)
School of Mechatronic Engineering, Xi'an Technological University,
No. 2, Xuefu Road, Xi'an, Shannxi, 710021, P. R. China
E-mail: junningli@outlook.com

Ka HAN, Mechanical Engineering
School of Mechatronic Engineering, Xi'an Technological University,
No. 2, Xuefu Road, Xi'an, Shannxi, 710021, P. R. China
E-mail: xatuhk@126.com

Qian WANG, Mechanical Engineering
School of Mechatronic Engineering, Xi'an Technological University,
No. 2, Xuefu Road, Xi'an, Shannxi, 710021, P. R. China
E-mail: xatuqianw@163.com

Wuge CHEN, Mechanical Engineering
School of Mechatronic Engineering, Xi'an Technological University,
No. 2, Xuefu Road, Xi'an, Shannxi, 710021, P. R. China
E-mail: wgchen2018@126.com

Jiafan XUE, Mechanical Engineering
School of Mechatronic Engineering, Xi'an Technological University,
No. 2, Xuefu Road, Xi'an, Shannxi, 710021, P. R. China
E-mail: xatujiapanxue@163.com